Original Paper

Energy consumption in the glass melting process

Part 2. Results of calculations[1])

Lubomír Němec

Laboratory of Glass and Ceramic Materials of the Institute of Chemical Technology and Academy of Sciences of Czech Republic, Prague (Czech Republic)

A simple model melting space of 1 m^3 has been proposed to demonstrate the influence of internal melting factors such as temperature, pressure, glass composition, size distribution in batch and glass flow distribution, on the specific energy consumption of the glass melting process. The laboratory data have been applied to evaluate the constants in proposed relations expressing this influence. The numerical results are graphically presented and show the main tendencies in the energy consumption development; the upper limits of the high-temperature application are obvious as well as the promising role of glass stirring, glass flow distribution and the physical way of refining.

Energieverbrauch beim Glasschmelzprozeß
Teil 2. Ergebnisse der Berechnungen

An einem einfachen Modell mit einem Schmelzvolumen von 1 m^3 wird der Einfluß innerer Schmelzfaktoren, wie Temperatur, Druck, Glaszusammensetzung, Korngröße des Gemenges und Glasströmungsverteilung, auf den spezifischen Energieverbrauch des Glasschmelzprozesses aufgezeigt. Mit Hilfe der in Laborversuchen gewonnenen Daten werden die Konstanten der angenommenen Beziehungen zwischen dem spezifischen Energieverbrauch und den genannten Schmelzfaktoren abgeschätzt. Die numerisch gewonnenen Ergebnisse werden grafisch dargestellt und zeigen die hauptsächlichen Entwicklungstendenzen des Energieverbrauchs; es sind sowohl die oberen Grenzen für die Anwendung hoher Temperaturen erkennbar als auch die vielversprechende Rolle, die das Rühren des Glases, die Glasströmungsverteilung und die physikalische Läuterung spielt.

1. Introduction

The specific energy consumption is an important characteristic of the glass melting process, and its prediction when varying the melting conditions is a significant task for the process modelling. At present, however, no complex model at disposal is able to describe the real influence of all internal factors of the process or to apply laboratory results to the model of the melting equipment. In Part 1 of this paper [1], the simple formula for the specific energy consumption has been presented, including the time factor of the melting process. Using a simplified model of the melting process, simple theoretical equations and experimental data of the author as well as from literature, relations have been derived, facilitating the expression of the influence of the internal melting factors – such as temperature, pressure, glass composition, size distribution in the batch and glass stirring – on the course of the melting process. If the simple mathematical or the liquid model of the melting space is simultaneously at disposal providing the fundamental information about glass flow, i.e. the critical and average residence time, dead volume and average temperatures, the qualified estimation of energy consumption when varying the melting factors may be performed. This part of the work presents the results of calculations of the specific energy consumption and their derivatives using the mentioned relations from [1] and available experimental data in a model melting space.

Received July 25, 1994, revised manuscript October 17, 1994.

[1]) Part 1, Theoretical relations. Glastech. Ber. Glass Sci. Technol. **68** (1995) no. 1, p. 1–10.

2. Model melting space

In order to express the influence of the internal melting factors on the specific energy consumption, H_M^0, numerically, the simple experimental melting space has been proposed having no energy recycling and being surrounded by two layers of refractory materials. The inner melting space has a volume of 1 m^3, the thickness of both refractory walls is 0.2 m. The details are obvious from figure 1. The refractory material (zone no. 1) in the inner layer is the corundum baddeleyite with $\lambda_1 = -1.37\,(1-4.03 \cdot 10^{-3}\,T)$ and that in the outer layer (zone no. 2) is compact fireclay material with $\lambda_2 = 0.7 + 0.64 \cdot 10^{-3}\,T$ (λ in $W\,m^{-1}\,K^{-1}$) [2]. For reasons of simplicity, $T^{max} = \bar{T} = T_1$, i.e. $\alpha' = \beta = 1$, and $T_3 = T^{ex} = 373$ K. The temperature dependence of λ_1 and λ_2 as well as the specific heat losses through the boundaries, $\dot{H}_A^L$, are presented in figure 2. The temperature dependence of the term $C^G\,(T^{max} - T^e)$ [1, equation (4)] for the soda–lime–silica glass (composition in wt%: 74 SiO_2, 16 Na_2O, 10 CaO) is plotted in figure 3.

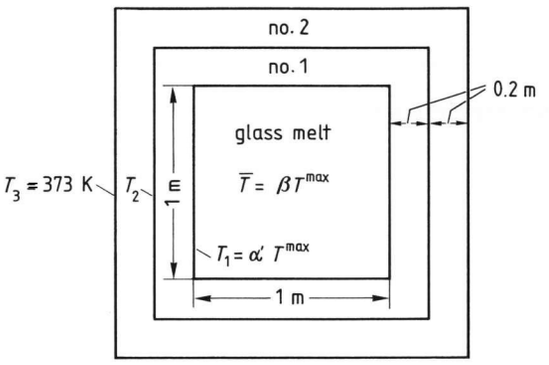

Figure 1. Scheme of the model melting space for the calculation of the specific energy consumption, H_M^0. Zone no. 1: corundum–baddeleyite material (ER 1681), zone no. 2: compact fireclay material.

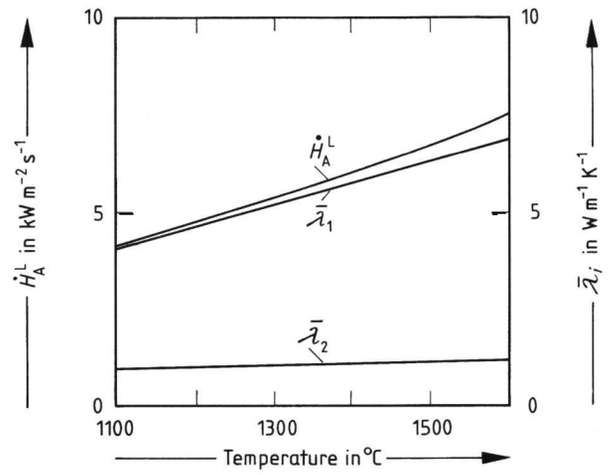

Figure 2. Dependence of the average heat conductivity of the ER 1681 material, $\bar{\lambda}_1$, the compact fireclay material, $\bar{\lambda}_2$, and the specific heat flow through the boundary, $\dot{H}_A^L$, on temperature.

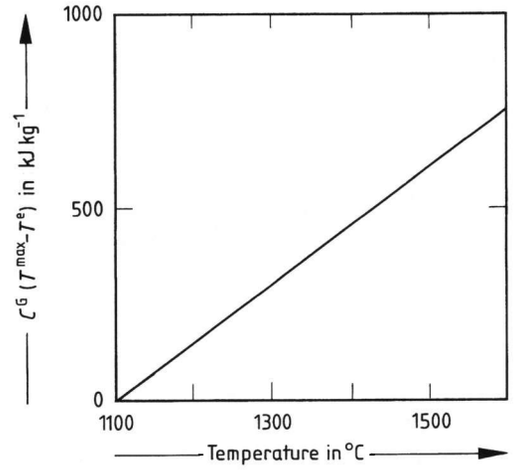

Figure 3. Dependence of the energy necessary to heat the model soda–lime–silica glass (composition in wt%: 74 SiO_2, 16 Na_2O, 10 CaO) from the exit temperature, T^e, to its maximum value, T^{max}, on the temperature. T^e = 1373 K, H_M^G = = 2100 kJ kg^{-1}.

The small changes of heat capacity, C^G, and density with the composition changes of glass have been neglected in the calculations of H_M^0.

3. Experimental data and results of calculations

When investigating the influence of temperature [1, section 4.1.] and the melting process being controlled by sand dissolution, i.e., $\tau_{Me}^{Cr} = \tau_D^{Cr}$, where τ_{Me}^{Cr} and τ_D^{Cr} are the required melting time and the sand dissolution time on the critical path, respectively, the laboratory experimental and interpolated values of τ_D for the soda–lime–silica glass have been applied [3]. As is obvious from figure 4a, there is a good agreement between these data and the proposed temperature dependence given in [1, equation (12)] which has the concrete form:

$$\tau_D^{Cr} = 7.74 \cdot 10^4 \exp\left(\frac{2.82 \cdot 10^4}{T^{max}} - 19.18\right) \qquad (1)$$

where $T^{max} \langle 1373; 1873\ K \rangle$. If the melting process is controlled by refining, i.e. $\tau_{Me}^{Cr} = \tau_R^{Cr} =$ where τ_R^{Cr} is the refining time on critical path = the experimental values of τ_R^{Cr} (being obtained using the simplified equation for τ_R and experimental values of gas concentrations, solubilities and their diffusion coefficients in float glass [4, table 3]) have been applied to express the numerical form of equation (18) in Part 1:

$$\tau_R^{Cr} = 1.07 \cdot 10^{-12} \exp \frac{5.84 \cdot 10^4}{T^{max}} \qquad (2)$$

where $T^{max} \in \langle 1523\ K;\ 1773\ K \rangle$, $h_o = 1$ m, a_o (initial bubble radius) = $5 \cdot 10^{-4}$ m.

In figure 4b is plotted the temperature dependence of H_M^0 [1, equation (13)] for the different values of $K^{Cr}/(1-m)$ and $\tau_{Me}^{Cr} = \tau_D^{Cr}$ as well as for $\tau_{Me}^{Cr} = \tau_R^{Cr}$. The corresponding values of $\partial H_M^0/\partial T^{max}$ [1, equation (14)] are plotted in figure 4c.

When investigating the influence of external pressure on the melting behaviour (see section 4.2. in Part 1), only the case $\tau_{Me}^{Cr} = \tau_R^{Cr}$ has been considered. The values of τ_R^{Cr} have been obtained using the experimental and calculated values of bubble growth rates at different pressures [5] and a temperature of 1400 °C. The glass was TV glass refined by 0.55 wt% Sb_2O_3 and 1.8 wt% K_2O (as KNO_3) or TV glass without any refining agent. Equation (20) in Part 1 has the concrete forms:

– for the case with refining agents:

$$\tau_R^{Cr} = \frac{1}{\left(\frac{1.76 \cdot 10^{-3}}{p_{ex}} - 1.66 \cdot 10^{-5}\right)^{2/3}} \qquad (3)$$

with $p_{ex} \in \langle 1\ kPa;\ 100\ kPa \rangle$;

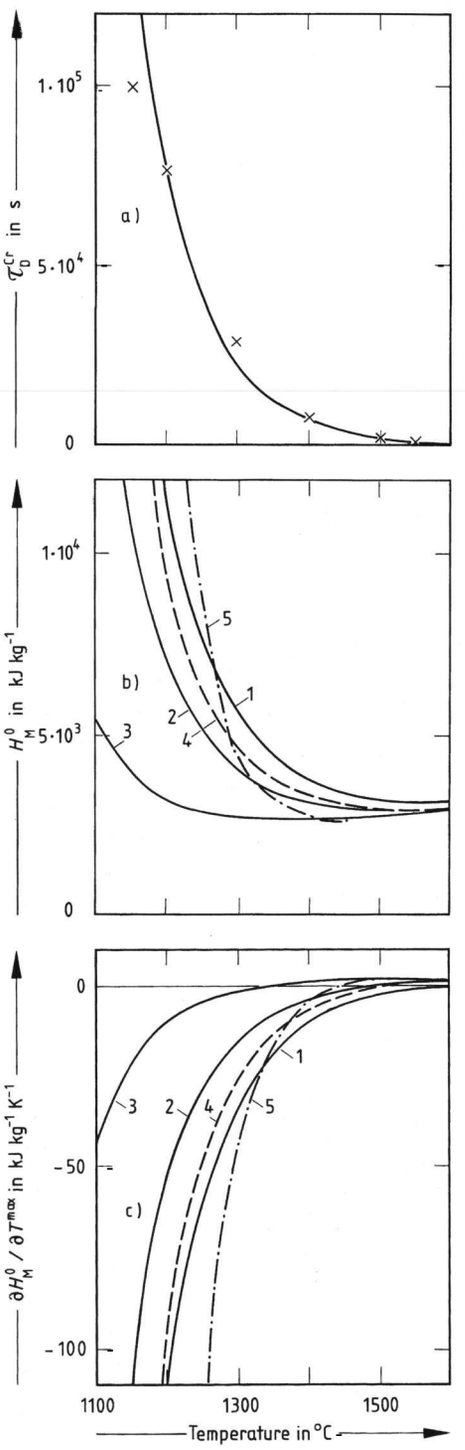

Figures 4a to c. Influence of temperature on the specific energy consumption.
a) Dependence of the sand dissolution time, τ_D^{Cr}, on temperature for the model glass refined by 0.7 wt% Na_2O as Na_2SO_4, $r_{max\,o} = 2.5 \cdot 10^{-4}$ m. ——: proposed equation (1), ×: experimental and interpolated values.
b) Dependence of the specific energy consumption, H_M^0, for the model soda–lime–silica glass on temperature, $\tau_{Me}^{Cr} \equiv \tau_D^{Cr}$; curve 1: $K^{Cr}/(1-m) \equiv 10$, curve 2: $K^{Cr}/(1-m) \equiv 5$, curve 3: $K^{Cr}/(1-m) \equiv 1$, curve 4: $K^{Cr} \equiv 5$, $\partial m/\partial T^{max} \equiv -1 \cdot 10^{-3}\,K^{-1}$, $m = 0.5$ at 1100 °C, curve 5: same dependence for float glass, $\tau_{Me}^{Cr} \equiv \tau_R^{Cr}$, $K^{Cr}/(1-m) = 10$.
c) Relation between $\partial H_M^0/\partial T^{max}$ and temperature at the same conditions as in figure 4b.

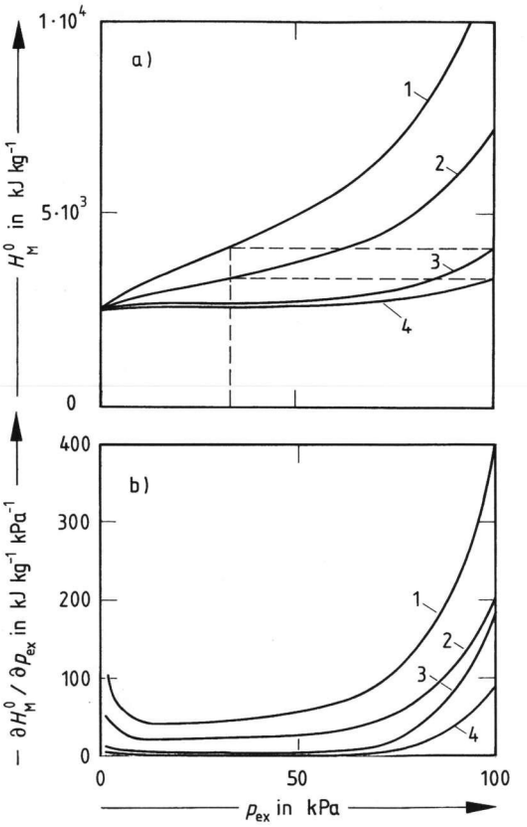

Figures 5a and b. Influence of external pressure on the specific energy consumption for the TV glass at 1400 °C, $h_o = 0.25$ m, $a_o = 1 \cdot 10^{-4}$ m, $\tau_{Me}^{Cr} = \tau_R^{Cr}$.
a) Dependence of H_M^0 on external pressure; curve 1: $K^{Cr}/(1-m) = 10$, without refining agents, curve 2: $K^{Cr}/(1-m) = 5$, without refining agents, curve 3: $K^{Cr}/(1-m) = 10$, with refining agents, curve 4: $K^{Cr}/(1-m) = 5$, with refining agents.
b) Relation between $\partial H_M^0/\partial p_{ex}$ and external pressure at the same conditions as in figure 5a.

– for the case without refining agents:

$$\tau_R^{Cr} = \frac{1}{\left(\dfrac{4.73 \cdot 10^{-5}}{p_{ex}} - 4.01 \cdot 10^{-7}\right)^{2/3}} \tag{4}$$

with $p_{ex} \in \langle 1\,kPa;\ 100\,kPa \rangle$. The pressure dependence of H_M^0 is then presented in figure 5a and the corresponding dependence of $\partial H_M^0/\partial p_{ex}$ in figure 5b (see equations (21 and 22) in Part 1).

The case when $\tau_{Me}^{Cr} \equiv \tau_D^{Cr}$ and the concentrations of major glass components are varying (see section 4.3.1. and equation (24) in Part 1), is represented by the batch-free times obtained by Potts [6 and 7]. The following concrete forms of equation (24) (Part 1) are valid:

$$\tau_D^{Cr} = \frac{38.34}{0.777 - w_{SiO_2}} \tag{5}$$

where $w_{SiO_2} \in \langle 0.695;\ 0.77 \rangle$ and equation (5) is valid for the Na_2O–CaO–MgO–SiO_2 glass (14 wt% CaO + MgO)

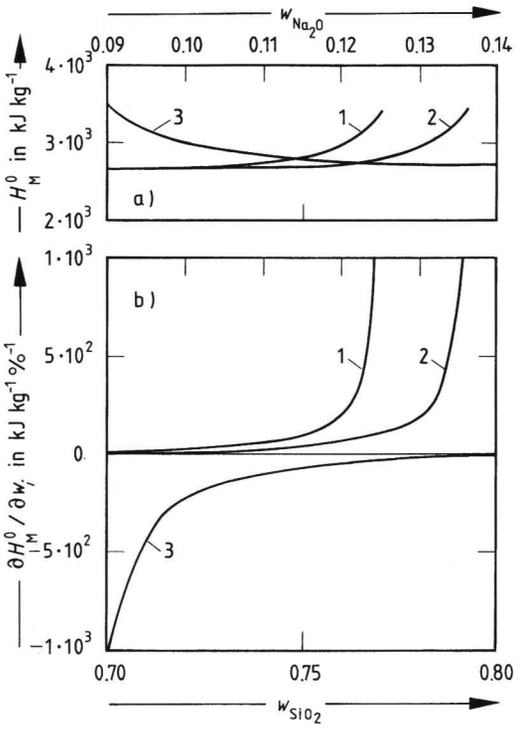

Figures 6a and b. Influence of major glass components on the specific energy consumption; $\tau^{Cr}_{Me} = \tau^{Cr}_D$, temperature 1427 °C.
a) Dependence of H^0_M on the glass composition; curve 1: $K^{Cr}/(1-m) = 10$, see equation (5), curve 2: $K^{Cr}/(1-m) = 10$, see equation (6), curve 3: $K^{Cr}/(1-m) = 10$, see equation (7).
b) Relation between $\partial H^0_M/\partial w_i$ and the glass composition at the same conditions as in figure 6a.

at 1427 °C whereas the corresponding dependence in the soda–lime–silica glass (10 wt% CaO) at the same temperature is given by:

$$\tau^{Cr}_D = \frac{43.2}{0.800 - w_{SiO_2}} \tag{6}$$

with $w_{SiO_2} \in \langle 0.708; 0.792\rangle$. Both equations (5 and 6) attribute the total change of τ^{Cr}_D only to the changes of w_{SiO_2}. If the composition changes are not accompanied by the variation of w_{SiO_2}, only changes of the coefficient of mass transfer, α, may be expected. The proposed equation using some experimental results by Potts [7] and considering the substitution B_2O_3 for Na_2O has the form:

$$\tau^{Cr}_D = \frac{43.7}{w_i - 8.17 \cdot 10^{-2}} \tag{7}$$

where $w_i \equiv w_{Na_2O} \in \langle 0.09; 0.135\rangle$ and $\bar{\alpha}$ is expected to be proportional to $w_i - 8.17 \cdot 10^{-2}$. The relation between H^0_M and w_i according to equation (25) in Part 1 is shown in figure 6a and the corresponding values of $\partial H^0_M/\partial w_i$ (see equation (26) in Part 1) in figure 6b.

The influence of variations of major glass components on the refining time has been published by Lyle [8]. The application of his experimental refining times at 1475 °C to obtain the concrete forms of equations (28 and 29) in Part 1 gives:

– for the soda–lime–silica glasses (10 wt% CaO) without refining agents:

$$\tau^{Cr}_R \equiv 8.82 \cdot 10^4 w_{SiO_2} - 6.24 \cdot 10^4 \tag{8}$$

with $w_{SiO_2} \in \langle 0.72; 0.78\rangle$ and

– for the case of 0.3 % SO_3 present in the same soda–lime–silica glasses:

$$\tau^{Cr}_R = \frac{1}{\left(\dfrac{4.95 \cdot 10^{-6}}{w_{Na_2O}} - 2.58 \cdot 10^{-5}\right)^{2/3}} \tag{9}$$

with $w_{Na_2O} \in \langle 0.115; 0.189\rangle$. The corresponding values of H^0_M and $\partial H^0_M/\partial w_i$ (see equations (30 and 31) in Part 1) are shown in figures 7a and b.

When the concentrations of refining agents Na_2SO_4, NaCl and As_2O_3, respectively, are varied (see section 4.3.2. in Part 1) and the melting process is controlled by the sand dissolution, $\tau^{Cr}_{Me} = \tau^{Cr}_D$, the experimental and interpolated results of τ_D from [3] have been applied.

The concrete dependence of equation (39) in Part 1 have the following forms:

$$\tau^{Cr}_D \equiv 8.90 \cdot 10^6 w_{Na_2O} + 2.1 \cdot 10^4 \tag{10}$$

with w_{Na_2O} as $Na_2SO_4 \in \langle 0; 0.01\rangle$;

$$\tau^{Cr}_D = 8.93 \cdot 10^6 w_{Na_2O} + 1.2 \cdot 10^4 \tag{11}$$

with w_{Na_2O} as NaCl $\in \langle 0; 0.03\rangle$ and

$$\tau^{Cr}_D = 1.50 \cdot 10^6 w_{As_2O_3} + 3.2 \cdot 10^4 \tag{12}$$

with $w_{As_2O_3} \in \langle 0; 0.03\rangle$. Equations (10 to 12) are valid at 1200 °C and equation (13)

$$\tau^{Cr}_D = -1.77 \cdot 10^5 w_{Na_2O} + 2.7 \cdot 10^3 \tag{13}$$

with w_{Na_2O} as $Na_2SO_4 \in \langle 0; 0.01\rangle$ is valid for the temperature 1500 °C. As is obvious from equation (13), the relatively complicated relation between τ^{Cr}_D and w_i at high temperatures (see equation (38) in Part 1) has been approximated by the decreasing straight line. The corresponding dependence of H^0_M on the concentrations of refining agent (see equation (40) in Part 1) is presented in figure 8a, whereas the temperature dependence of $\partial H^0_M/\partial w_{Na_2O}$ for sodium sulphate (see equation (41) in Part 1) is plotted in figure 8b. The results are completed by showing the relation between $\partial \tau^{Cr}_D/\partial w_{Na_2O}$ (Na_2O as Na_2SO_4) and temperature in figure 8c.

When the melting process is controlled by refining, $\tau^{Cr}_{Me} = \tau^{Cr}_R$, the dependence of refining time on the refining agent concentration is given by equation (32) in

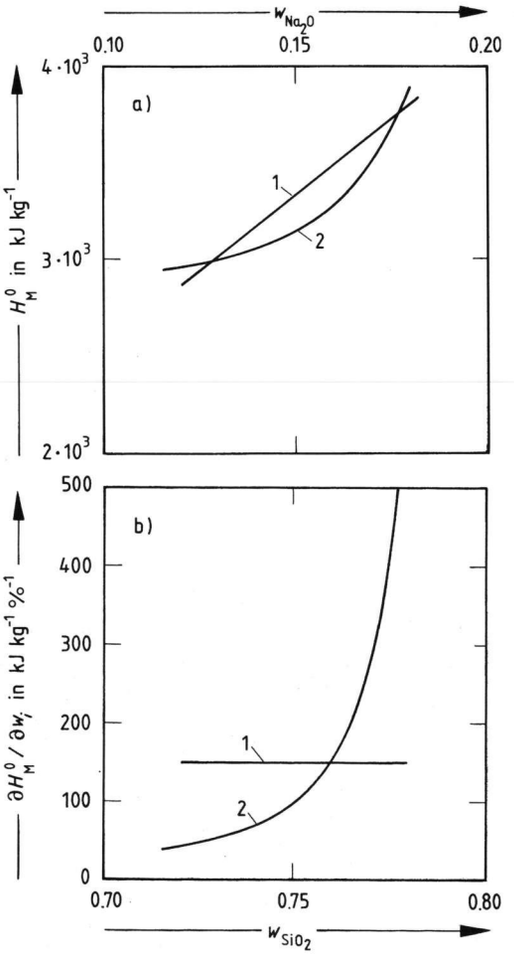

Figures 7a and b. Influence of major glass components on the specific energy consumption; $\tau_{Me}^{Cr} = \tau_R^{Cr}$, soda–lime–silica glass (CaO = 10 wt%), temperature 1475 °C.
a) Dependence of H_M^0 on the glass composition; curve 1: $K^{Cr}/(1-m) = 10$, without refining agents, see equation (8), curve 2: $K^{Cr}/(1-m) = 10$, with refining agents, see equation (9).
b) Relation between $\partial H_M^0/\partial w_i$ and the glass composition at the same conditions as in figure 7a.

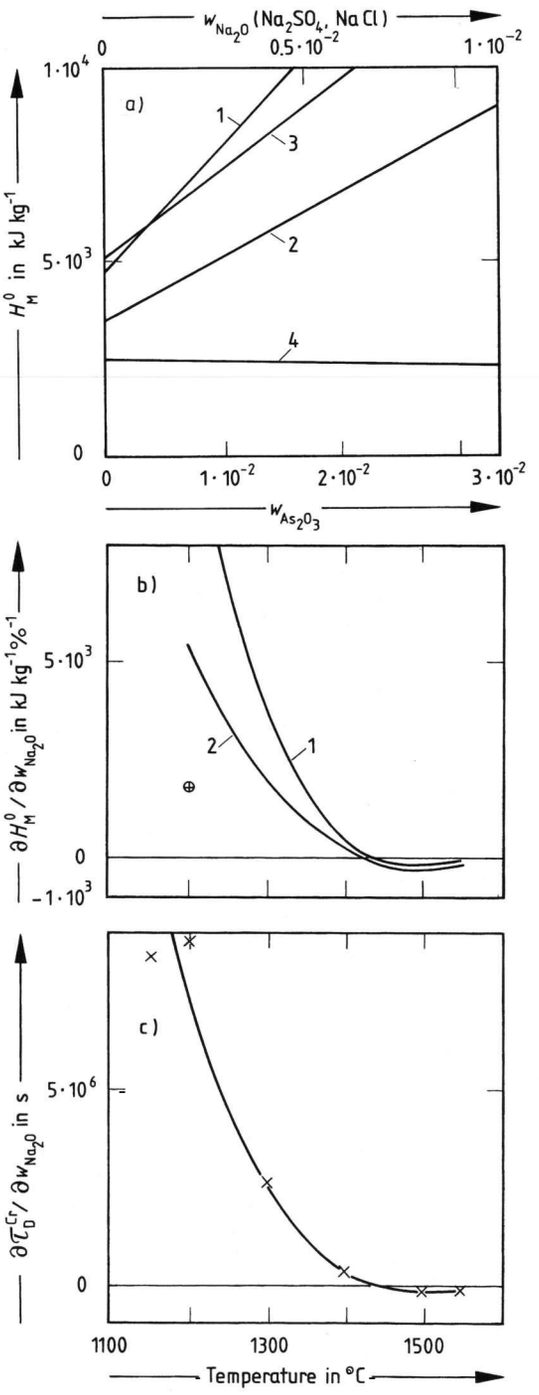

Figures 8a to c. Influence of refining agents on the specific energy consumption, $\tau_{Me}^{Cr} = \tau_D^{Cr}$, $r_{max\,o} = 2.5 \cdot 10^{-4}$ m, model glass (composition in wt%: 74 SiO_2, 16 Na_2O, 10 CaO).
a) Dependence of H_M^0 on the refining agent additions; curve 1: Na_2O as Na_2SO_4, $K^{Cr}/(1-m) = 10$, temperature 1200 °C, see equation (10), curve 2: Na_2O as NaCl, $K^{Cr}/(1-m) = 5$, temperature 1200 °C, see equation (11), curve 3: As_2O_3 + $NaNO_3$, $K^{Cr}/(1-m) = 10$, temperature 1200 °C, see equation (12), curve 4: Na_2O as Na_2SO_4, $K^{Cr}/(1-m) = 10$, temperature 1500 °C, see equation (13).
b) Relation between $\partial H_M^0/\partial w_i$ and temperature; curve 1: w_i = = Na_2O as Na_2SO_4, $K^{Cr}/(1-m) = 10$, curve 2: w_i = Na_2O as Na_2SO_4, $K^{Cr}/(1-m) = 5$, ⊕: $\partial H_M^0/\partial w_{As_2O_3}$ at 1200 °C, $K^{Cr}/(1-m) = 10$.
c) Relation between $\partial \tau_D^{Cr}/\partial w_i$ and temperature for sodium sulphate as refining agent (0.7 wt% Na_2O as Na_2SO_4).

Part 1. Applying the values of τ_R^{Cr} obtained from experimental values of bubble growth rates [9] for As_2O_3 + + $NaNO_3$ gives the concrete forms of equation (32) (Part 1):

$$\tau_R^{Cr} = \frac{8.62 \cdot 10^{-2}}{(4.22 \cdot 10^{-5}\, w_{As_2O_3} + 2.50 \cdot 10^{-9})^{2/3}} \qquad (14)$$

with $w_{As_2O_3} \in \langle 0;\ 0.03 \rangle$ at the temperature of 1400 °C and:

$$\tau_R^{Cr} = \frac{7.29 \cdot 10^{-2}}{(8.74 \cdot 10^{-5}\, w_{As_2O_3} + 2.5 \cdot 10^{-9})^{2/3}} \qquad (15)$$

with $w_{As_2O_3} \in \langle 0;\ 0.04 \rangle$ at the temperature of 1450 °C. Equation (32) from Part 1 is almost precisely fulfilled at 1450 °C. The corresponding values of H_M^0 from equation

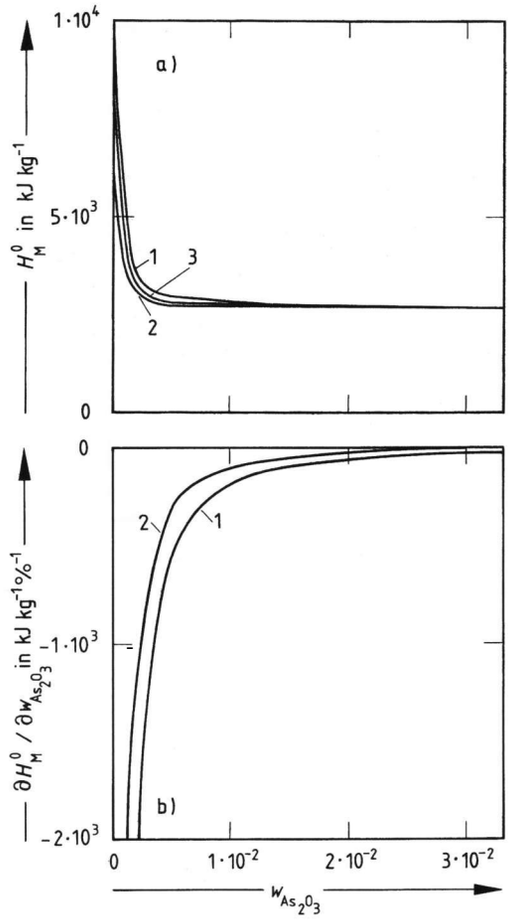

Figures 9a and b. Influence of refining agents on the specific energy consumption, $\tau_{Me}^{Cr} = \tau_R^{Cr}$, model glass (composition in wt%: 74 SiO_2, 16 Na_2O, 10 CaO).
a) Dependence of H_M^0 on the As_2O_3 + $NaNO_3$ additions; curve 1: 1400 °C, $K^{Cr}/(1-m)$ = 10, see equation (14), curve 2: 1400 °C, $K^{Cr}/(1-m)$ = 5, see equation (14), curve 3: 1450 °C, $K^{Cr}/(1-m)$ = 10, see equation (15).
b) Relation between $\partial H_M^0/\partial w_{As_2O_3}$ and As_2O_3 + $NaNO_3$ additions; curve 1: 1400 °C, $K^{Cr}/(1-m)$ = 10, curve 2: 1450 °C, $K^{Cr}/(1-m)$ = 10.

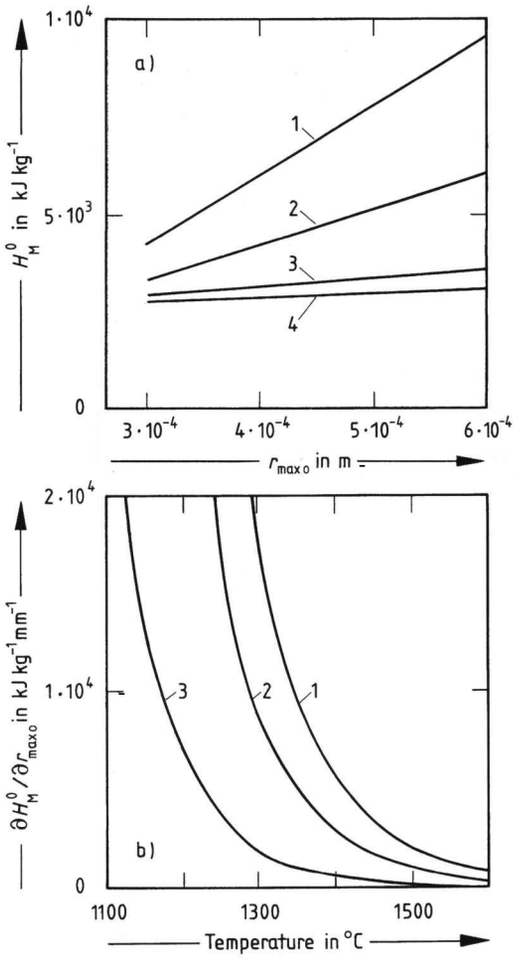

Figures 10a and b. Influence of the maximum sand particle size, $r_{max\,o}$, on the specific energy consumption in the float glass, $\tau_{Me}^{Cr} = \tau_D^{Cr}$.
a) Dependence of H_M^0 on the maximum sand particle size; curve 1: 1300 °C, $K^{Cr}/(1-m)$ = 10, curve 2: 1300 °C, $K^{Cr}/(1-m)$ = 5, curve 3: 1500 °C, $K^{Cr}/(1-m)$ = 10, curve 4: 1500 °C, $K^{Cr}/(1-m)$ = 5.
b) Relation between $\partial H_M^0/\partial r_{max\,o}$ and temperature for the float glass; curve 1: $K^{Cr}/(1-m)$ = 10, curve 2: $K^{Cr}/(1-m)$ = 5, curve 3: $K^{Cr}/(1-m)$ = 1.

(33) in Part 1 are plotted in figure 9a whereas figure 9b presents the appropriate values of $\partial H_M^0/\partial w_{As_2O_3}$.

Investigating the size distribution of batch (see section 4.4. in Part 1), only the influence of size distribution of sand on the sand dissolution process, $\tau_{Me}^{Cr} = \tau_D^{Cr}$, has been considered. If the sizes of individual raw materials match, the dependence of melting time on maximum sand particle (see section 4.4.1. in Part 1) may be expressed by equation (44) in Part 1. In the calculations, the experimental values of τ_D for float glass have been used [10]. The maximum sand particle, $r_{max\,o}$, was $5 \cdot 10^{-4}$ m. The appropriate values of τ_D for $r_{max\,o}$ = $= 3 \cdot 10^{-4}$ m have been interpolated. The concrete form of equation (44) (Part 1, involving the temperature dependence of τ_D) is:

$$\tau_D^{Cr} = 7.96 \cdot 10^{-2} \exp\left(\frac{3.33 \cdot 10^4}{T^{max}}\right)(r_{max\,o} - 2 \cdot 10^{-4}) \quad (16)$$

with $T^{max} \in \langle 1373\,K; 1873\,K\rangle$, $r_{max\,o} \geq 3 \cdot 10^{-4}$ m. The resulting dependencies of H_M^0 on $r_{max\,o}$ for the temperatures 1300 and 1500 °C, respectively, are presented in figure 10a, whereas the temperature dependence of $\partial H_M^0/\partial r_{max\,o}$ is plotted in figure 10b.

A similar case may be cited from the work of Potts, Brookover and Burch [11], where the linear relation between τ_D^{Cr} and $r_{max\,o}$ at 1427 °C could be expressed as: $\tau_D^{Cr} = 6.86 \cdot 10^7 r_{max\,o} - 4.21 \cdot 10^3$, $r_{max\,o} \geq 1 \cdot 10^{-4}$ m. The resulting values of H_M^0 as well as $\partial H_M^0/\partial r_{max\,o}$ are summarized in table 1.

When the sand particle distribution varies keeping the value of $r_{max\,o}$ constant (see section 4.4.2. in Part 1) equation (48) in Part 1 has been proposed. Using the values of τ_D for monodisperse sand and the same values for the industrial sand in float glass [12], the concrete forms of equation (48) are:

Table 1. Values of H_M^0 and $\partial H_M^0/\partial r_{max\,o}$, obtained using experimental data by [11]

$r_{max\,o}$ in m	H_M^0 in kJ/kg		$\partial H_M^0/\partial r_{max\,o}$ in kJ/(kg mm)	
	$K^{Cr}/(1-m) = 5$	$K^{Cr}/(1-m) = 10$	$K^{Cr}/(1-m) = 5$	$K^{Cr}/(1-m) = 10$
$1 \cdot 10^{-4}$	2805	3020	$5.55 \cdot 10^3$	$1.11 \cdot 10^4$
$2 \cdot 10^{-4}$	3360	4130		
$3 \cdot 10^{-4}$	3915	5240		

– at 1300 °C:

$$\tau_D^{Cr} \equiv 5.33 \cdot 10^4 - 2.60 \cdot 10^7 r_{io} \quad (17)$$

with $r_{io} \in \langle 0;\ 5 \cdot 10^{-4}\,\mathrm{m}\rangle$ and

– at 1200 °C:

$$\tau_D^{Cr} \equiv 2.15 \cdot 10^5 - 1.48 \cdot 10^8 r_{io} \quad (18)$$

with $r_{io} \in \langle 0;\ 5 \cdot 10^{-4}\,\mathrm{m}\rangle$. r_{io} is the size of the most frequent sand particle on the very sharp size distribution curve. The appropriate values of H_M^0 as well as the temperature dependence of $\partial H_M^0/\partial r_{io}$ are presented in figures 11a and b.

The experimental results of Potts, Brookover and Burch [11] show a linear decrease of the batch-free time with cullet concentration when commercial batch components were used. The dependence of τ_D^{Cr} at 1427 °C for the SiO_2–Al_2O_3–CaO–MgO–R_2O glass has the concrete form:

$$\tau_D^{Cr} \equiv 9.3 \cdot 10^3 - 1.80 \cdot 10^4 w_{cul} \quad (19)$$

with $w_{cul} \in \langle 0;\ 0.3\rangle$. The appropriate values of H_M^0 and $\partial H_M^0/\partial w_{cul}$ are presented in table 2.

In order to express the influence of glass convection on the course of the melting process, i.e. on $\tau_{Me}^{Cr} \equiv \tau_D^{Cr}$ (see section 4.5. in Part 1), equations (51 and 52) in Part 1 have been proposed. As the value of grad v could not be measured in laboratory experiments, the proportionality between grad v and the amount of bubbling stirring gas has been assumed. Thus, the concrete forms of dependences between τ_D^{Cr} and $\dot{V}$ (volume flow of gas through the glass melt in ml · min^{-1}) are:

– for the temperature 1200 °C:

$$\tau_D^{Cr} = \frac{77\,000}{1 + 0.101\,\dot{V}} \quad (20)$$

with $\dot{V} \in \langle 0;\ 200\,\mathrm{ml \cdot min^{-1}}\rangle$ and

– for the temperature 1500 °C:

$$\tau_D^{Cr} \equiv \frac{2980}{1 + 0.068\,\dot{V}} \quad (21)$$

with $\dot{V} \in \langle 0;\ 200\,\mathrm{ml \cdot min^{-1}}\rangle$. The good coincidence between the temperature dependences of proposed and experimental curves ($\dot{V} = 30\,\mathrm{ml \cdot min^{-1}}$) is obvious from figure 12a. The calculated dependence of H_M^0 on the intensity of glass stirring is also given in figure 12a, the corresponding values of $\partial H_M^0/\partial \dot{V}$ in figure 12b (see equations (53 and 54) in Part 1, respectively). In figure 12c is plotted H_M^0 versus $K^{Cr}/(1-m)$, i.e., the case when only glass flow distribution is changing at constant value of τ_D^{Cr}. The corresponding temperature dependence of $\partial(H_M^0/\partial(K^{Cr}/(1-m))$ is presented in figure 12d.

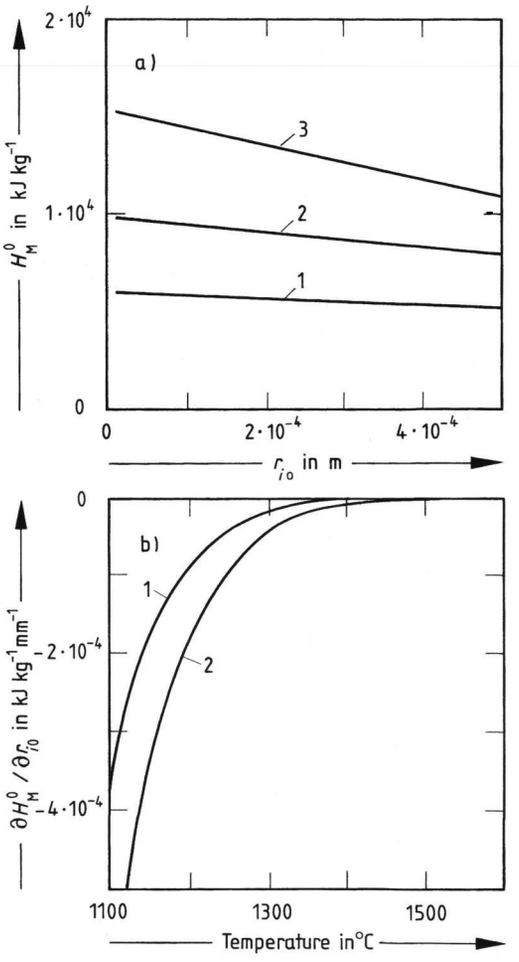

Figures 11a and b. Influence of the sand particle distribution on the specific energy consumption in the float glass, $r_{max\,o} = 5 \cdot 10^{-4}$ m, $\tau_{Me}^{Cr} = \tau_D^{Cr}$.
a) Dependence of H_M^0 on the size of the most frequent sand particle, r_{io}; curve 1: 1300 °C, $K^{Cr}/(1-m) = 5$, curve 2: 1300 °C, $K^{Cr}/(1-m) = 10$, curve 3: 1200 °C, $K^{Cr}/(1-m) = 5$.
b) Relation between $\partial H_M^0/\partial r_{io}$ and temperature for the float glass; curve 1: $K^{Cr}/(1-m) = 5$, curve 2: $K^{Cr}/(1-m) = 10$.

Table 2. Values of H_M^0 and $\partial H_M^0/\partial w_{cul}$, obtained using experimental data by [11]

w_{cul}	H_M^0 in kJ/kg		$\partial H_M^0/\partial w_{cul}$ in kJ/kg	
	$K^{Cr}/(1-m) = 5$	$K^{Cr}/(1-m) = 10$	$K^{Cr}/(1-m) = 5$	$K^{Cr}/(1-m) = 10$
0	3346	4103	1464	2928
0.1	3200	3810		
0.2	3005	3520		
0.3	2902	3224		

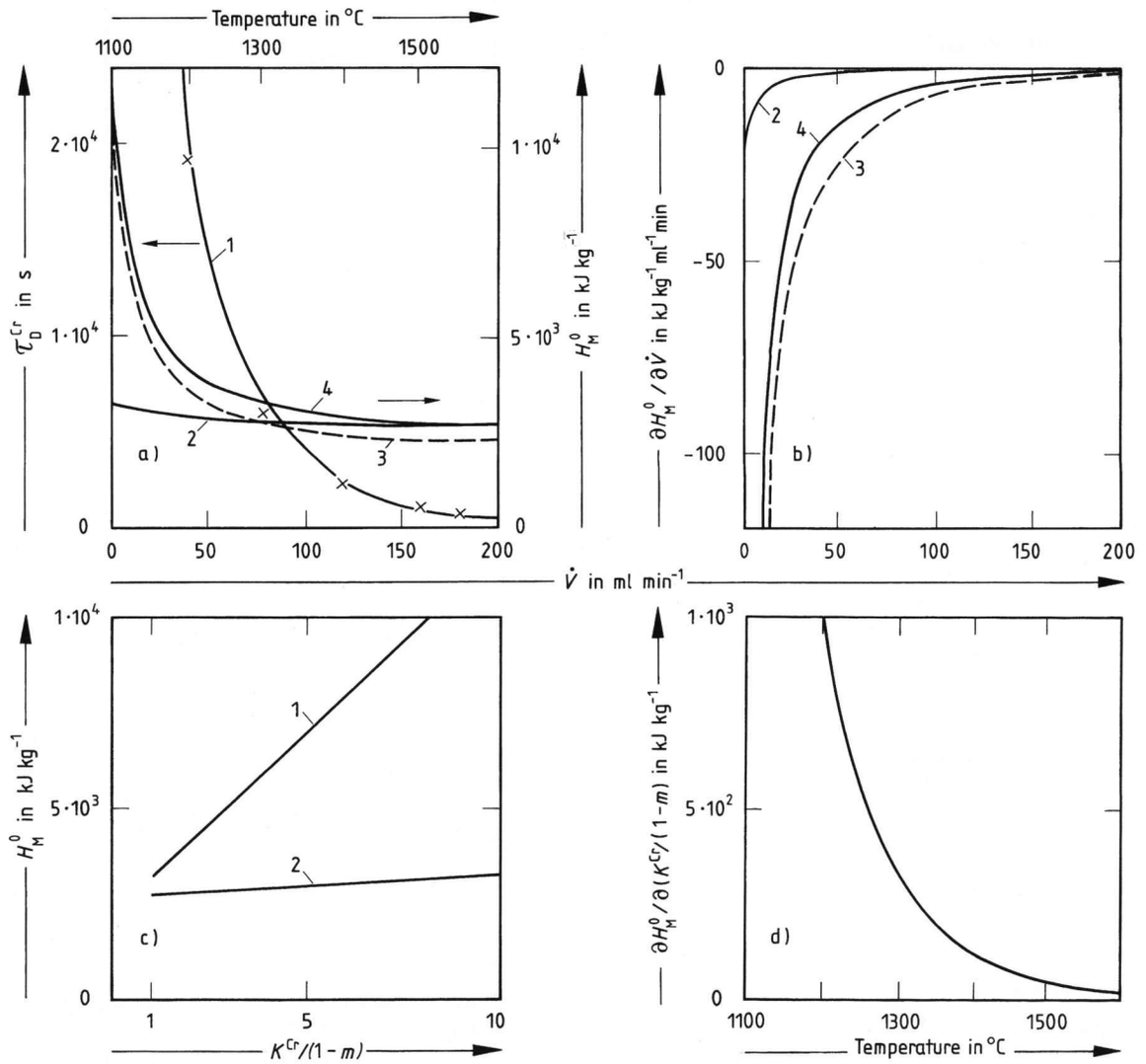

Figures 12a to d. Influence of the intensity of glass convection and glass flow distribution on the specific energy consumption in the model glass (composition in wt%: 74 SiO_2, 16 Na_2O, 10 CaO), 0.7 wt% Na_2O as Na_2SO_4, $r_{max\,o} = 2.5 \cdot 10^{-4}$ m, $\tau_{Me}^{Cr} = \tau_D^{Cr}$.
a) Relation between the sand dissolution time and temperature for the model glass being bubbled by 30 ml O_2 min^{-1}; curve 1: $\tau_D^{Cr} \equiv \exp\left(\frac{2.59 \cdot 10^4}{T^{max}} - 17.60\right)$, ×: experimental values, and dependence of H_M^0 on the glass convection intensity ($\dot{V}$); curve 2: 1500 °C, $K^{Cr}/(1-m) = 10$; curve 3: 1200 °C, $\partial K^{Cr}/\partial \dot{V} = -0.02$ min · ml^{-1}, $\partial m/\partial \dot{V} = -2.5 \cdot 10^{-3}$ min · ml^{-1}, $K^{Cr}/(1-m) = 10$ at $\dot{V} = 0$; curve 4: 1200 °C, $K^{Cr}/(1-m) = 10$.
b) Relation between $\partial H_M^0/\partial \dot{V}$ and the intensity of glass convection ($\dot{V}$) at the same conditions as in figure 12a.
c) Dependence of H_M^0 on the glass flow distribution ($K^{Cr}/(1-m)$) at constant value of τ_D^{Cr}, $\dot{V} = 0$; curve 1: 1200 °C, curve 2: 1500 °C.
d) Relation between $\partial H_M^0/\partial(K^{Cr}/(1-m))$ and temperature at constant value of τ_D^{Cr}.

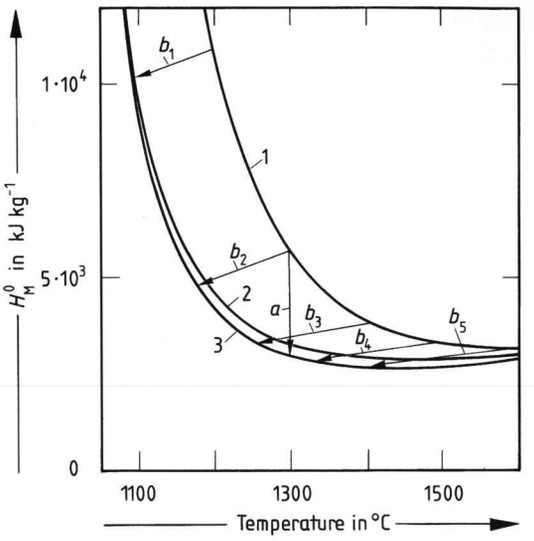

Figure 13. Decrease in specific energy consumption when applying the glass stirring by bubbling at laboratory conditions. Model glass (composition in wt%: 74 SiO_2, 16 Na_2O, 10 CaO), 0.7 wt% Na_2O as Na_2SO_4, $r_{max\,o} = 2.5 \cdot 10^{-4}$ m, $\tau_{Me}^{Cr} = \tau_D^{Cr}$. Curve 1: without stirring, $K^{Cr}/(1-m) = 10$, curve 2: stirred by bubbling ($\dot{V} = 30$ ml · min^{-1}), $K^{Cr}/(1-m) = 10$, curve 3: stirred by bubbling ($\dot{V} = 30$ ml · min^{-1}), $\partial(K^{Cr}/(1-m))/\partial T^{max} = -1.8 \cdot 10^{-2}$ K^{-1}, $K^{Cr}/(1-m) = 10$ at 1100 °C. *a*: increase of output at constant temperature, *b*: decrease of temperature at constant output ($\bar{\tau}$).

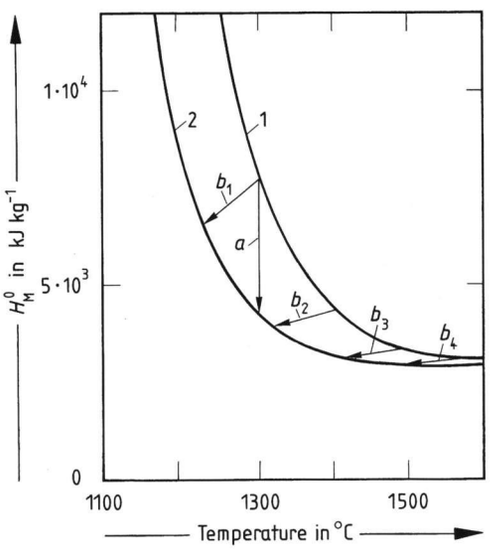

Figure 14. Decrease in specific energy consumption when removing the coarse portions of sand, float glass, $\tau_{Me}^{Cr} = \tau_D^{Cr}$, $K^{Cr}/(1-m) = 10$. Curve 1: $r_{max\,o} = 5 \cdot 10^{-4}$ m, curve 2: $r_{max\,o} = 3 \cdot 10^{-4}$ m. *a*: increase of output at constant temperature, *b*: decrease of temperature at constant output ($\bar{\tau}$).

Using already cited experimental and proposed dependences, the exploitation of melting reserve may be documented by the following results: In figure 13, there is shown how to exploit the melting reserve arisen from the glass stirring by bubbling. The analogous exploitation of the melting reserve arisen from the decrease of the maximum sand particle size is presented in figure 14.

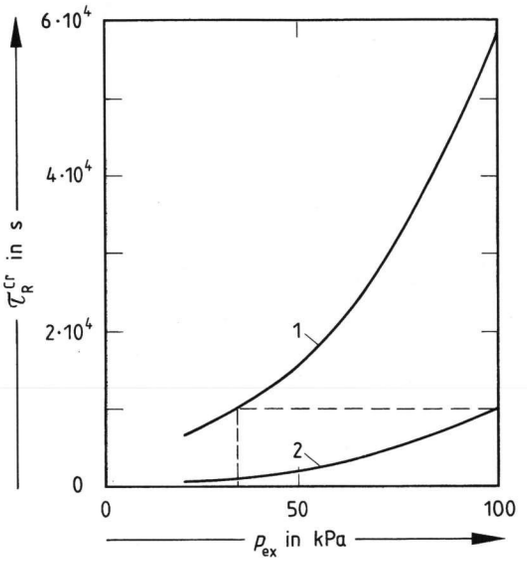

Figure 15. Dependence of refining time, τ_R^{Cr}, of TV glass on external pressure at 1400 °C, $a_o = 1 \cdot 10^{-4}$ m; $h_o = 0.25$ m. Curve 1: without refining agents, curve 2: with Sb_2O_3 + KNO_3 as refining agent.

Exploitation of the melting reserve – arising from the pressure decrease ($\tau_{Me}^{Cr} = \tau_R^{Cr}$) – for the melting without any refining agent is presented in figure 15. As the TV glass output must stay at a constant value in this case (see equation (6) in Part 1), the removing of refining agents at 1400 °C requires the pressure decrease from 100 to about 34 kPa (see also figure 5b).

4. Discussion of results

Temperature is the most important and most complex factor of the glass melting process. The steep decrease of energy consumption when increasing temperature (figure 4b) explains a well-known trend towards the application of very high melting temperatures during the last decades. However, an even further temperature increase proves to be inefficient as is obvious from equations (13 and 14) in Part 1 and from figures 4b and c. In figure 16 are plotted the partial derivatives of the specific energy consumption expressing the separated effect of temperature. As is obvious from this figure, the negative derivative $\partial H_M^\tau/\partial T^{max}$ expressing the decrease of melting time with temperature and the positive derivative $\partial H_M^T/\partial T^{max}$, expressing the increasing heat losses through the boundary, approach zero as $T^{max} \to \infty$. The value of C^G expressing the energy necessary for glass to be heated to the melting temperature is on the contrary positive and constant (if C^G is considered to be temperature-independent). At very high temperatures, the sum $\Sigma \partial H_M^i/\partial T^{max}$ is positive and the specific energy consumption grows with temperature. The smaller the heat losses are, the lower is the temperature of minimum energy consumption. This fact is demonstrated by figure 17, where the optimum melting temperature is plotted

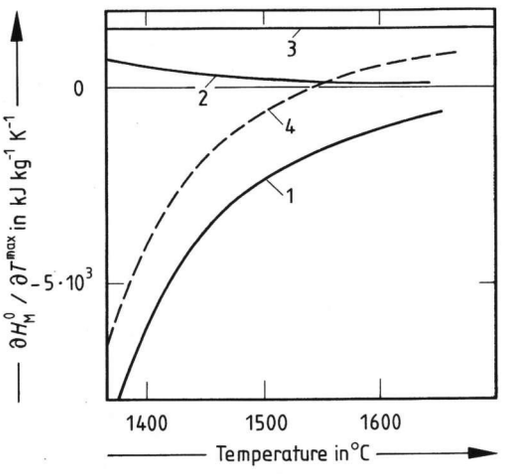

Figure 16. Relation between the single partial derivatives of H_M^0 and temperature for the model glass (composition in wt%: 74 SiO_2, 16 Na_2O, 10 CaO), 0.7 wt% Na_2O as Na_2SO_4, $r_{max\,o} = 2.5 \cdot 10^{-4}$ m, $\tau_{Me}^{Cr} = \tau_D^{Cr}$, $K^{Cr}/(1-m) = 5$.
Curve 1: $\partial H_M^T/\partial T^{max}$ = derivative of heat losses with temperature at constant heat flux through boundaries;
curve 2: $\partial H_M^T/\partial T^{max}$ = derivative of heat losses with temperature at constant melting time, τ_{Me}^{Cr};
curve 3: C^G;
curve 4: $\partial H_M^0/\partial T^{max}$.

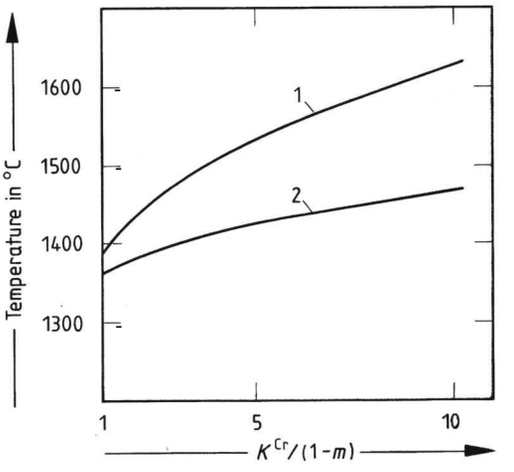

Figure 17. Dependence of the optimum melting temperature on the glass flow controlling ($K^{Cr}/(1-m)$). Curve 1: same glass as in figure 16, $\tau_{Me}^{Cr} = \tau_D^{Cr}$, curve 2: float glass, $a_o = 5 \cdot 10^{-4}$ m, $h_o = 1$ m, $\tau_{Me}^{Cr} = \tau_R^{Cr}$.

versus the value of $K^{Cr}/(1-m)$. With a very rational arrangement of the melting process, the melting temperature, therefore, need not to be extremely high. When refining is controlling the melting process, i.e., $\tau_{Me}^{Cr} = \tau_R^{Cr}$, the range of optimum temperatures almost coincides with the temperature interval of the efficiency of the refining agents (see curve 2 in figure 17).

The investigation of the influence of pressure has been restricted to the refining process and to the mechanism of bubble growth by diffusion of refining gas. As is obvious from figures 5a and b, especially the pressure region adjacent to normal pressure may be important from the energy point of view. Thus, even a slight pressure decrease in this region favourably influences the energy consumption, especially when the refining process at normal pressure is slow.

The usual variations of macroscopic glass components up to several percents do not seem to influence significantly the energy consumption when $\tau_{Me}^{Cr} \equiv \tau_D^{Cr}$. Excepted is the composition range adjacent to the equilibrium concentration of SiO_2 in the melt, where $\tau_D^{Cr} \to \infty$ and consequently $H_M^0 \to \infty$, (see curves 1 and 2 in figures 6a and b). If the concentration of SiO_2 in the final glass is constant, the composition variations reflect especially the viscosity changes as viscosity influences both the values of diffusion coefficients and the thickness of diffusion layer of SiO_2 on sand particle boundaries. Unfortunately, no general expression being able to predict quantitatively the effect of composition variation on the dissolution process has been available up to this time. When the melting process is controlled by refining, the energy consumption may be significantly affected as is seen from figures 7a and b; when no refining agents are added, only composition changes influencing viscosity are efficient (see curve 1 in figures 7a and b). In the presence of refining agents, the specific energy consumption may be very sensitive to the alkali content of glass as the refining effect decreases with increasing basicity of glass (see curve 2 in figures 7a and b).

The complex influence of refining agents on the dissolution process ($\tau_{Me}^{Cr} \equiv \tau_D^{Cr}$), described in [1, section 4.3.2.], is expressed in figures 8a and b. The presence of refining agents considerably increases the energy consumption at low temperatures or at a low degree of exploitation of a melting space. At high temperatures, however, the specific energy consumption slightly decreases with temperature due to a stirring effect of growing bubbles. As is obvious from figure 8b, the apparent effect of stirring bubbles ($\partial H_M^0/\partial w_{Na_2O} = 0$) occurs at about 1450 °C, where the bubble nucleation starts on sand particles [9] (see also figure 8c). If $\tau_{Me}^{Cr} = \tau_R^{Cr}$, the steep decrease of the specific energy consumption starts already at very low concentrations of refining agents. The further increase of refining agent additions is only slightly efficient from the energetic point of view. As is obvious from figures 9a and b, additions of As_2O_3 up to 0.5% are sufficient. This fact is in agreement with experience in practice.

The significance of removing coarse sand portions for the energy savings is well-known and the procedure is practically applied. As is obvious from figures 10a and b, the effect is more pronounced at lower temperatures and for a low exploitation of the melting space. The restriction of coarse sand portions represents probably the cheapest measure leading to energy savings in the glass melting process. The overall particle distribution, on the contrary, influences the energy consumption only

slightly; the sands with big portions of coarse particles (at given values of $r_{\max o}$) lead to lower energy consumptions as is obvious from figures 11a and b. The influence of sand size distribution on the refining behaviour is not involved in this approach.

Despite the problems connected with glass stirring devices in the full-scale melting equipments, the effect of this melting factor seems to be very promising. The energy consumption of the dissolution process steeply falls even at relatively low intensity of glass stirring as is obvious from figures 12a to d. When not only melting time but also the exploitation of the melting space is favourably influenced (see curve 3 in figure 12a), the specific energy consumption attains the very low values approaching the theoretical ones. Figures 12c and d presenting only the effect of the exploitation of the melting space on the energy consumption, show that the factor of glass flow influencing is particularly important. The most distinct disadvantage of glass stirring, however, is its frequently unclear and often unfavourable effect on glass refining and refractory wear.

The two possibilities of utilizing the melting reserve being plotted in figures 13 and 14 confirm that the only energy significant way is the output increase at constant temperature (see the abscissa $a \equiv \Delta H_M^0$ in both figures). The lower the melting temperature is, the more significant are the energy savings. The utilization of the melting reserve for the decrease in melting temperature (see the abscissa b_i in figures 13 and 14) leads only to small energy savings. With the exception of temperature, no energy savings are attainable when the favourable change of any melting factor is compensated by the less favourable change of another one as $(\partial H_M^0/\partial x_i)_{\bar{\tau}, T} = 0$.

5. Conclusion

Although the ascertained energy trends of the glass melting process are more or less qualitative, some conclusions may be useful for the process improvement and for the new conceptions of glass melting. The results show that the application of very high temperatures frequently reaches its limits from the energy point of view. In addition, some other factors, such as corrosion or volatilization, may restrict the application of very high temperatures. As for size distribution in the batch, the results of research leading to the restrictions of coarse batch portions and matching individual glass components are currently applied. When applying composition changes, the required glass properties must also be taken into account and this fact restricts the possible composition variations. As is obvious from the results, the refining process is more distinctly influenced by composition variations. The application of controlled glass stirring leads to the very low values of specific energy consumption for $\tau_{Me}^{Cr} \equiv \tau_D^{Cr}$, as $H_M^0 \rightarrow H_M^G$ if $\operatorname{grad} v \rightarrow \infty$. H_M^G involves here only enthalpy of chemical reactions, evaporation heats and modification heats as well as energy necessary to heat the glass from the ambient to exit temperature. At the same time, the application of physical ways of refining and separating both processes – sand dissolution and refining – appears to be one of the promising melting conceptions. The main technical problems arising here are the realization of refining (e.g., the low pressure chambers) and high energy supply in the area of batch heating and batch reactions. The attainment of the appropriate flow distribution in the melting space is a very interesting objective to be approached by mathematical modelling.

6. Nomenclature

6.1. Symbols

a	bubble radius in m
C	specific heat in $J\,kg^{-1}\,K^{-1}$
h	height of glass layer in m
H	energy consumption in J
$\dot{H}$	heat flow in $J\,s^{-1}$
K	constant
m	fraction of dead volume
p	pressure in Pa
r	radius of sand particle in m
T	temperature in K
$\bar{T}$	average temperature in K
v	velocity of glass flow in $m\,s^{-1}$
$\dot{V}$	gas volume flow in $ml\,min^{-1}$
w	mass fraction
α	coefficient of mass transfer in $m\,s^{-1}$
α'	constant
$\bar{\alpha}$	average value of the coefficient of mass transfer in $m\,s^{-1}$
β	constant
λ	heat conductivity in $W\,m^{-1}\,K^{-1}$
$\bar{\lambda}$	average heat conductivity in $W\,m^{-1}\,K^{-1}$
τ	time in s

6.2. Superscripts

Cr	critical value
e	exit value
ex	external value
G	value characterizing glass
i	indice relating to derivative of H_M
L	value characterizing heat losses
max	maximum value
0	overall value
T	value characterizing temperature
τ	value characterizing melting time

6.2. Subscripts

A	related to surface unit
cul	value characterizing cullet
D	dissolution
ex	external value
i	indice relating to glass component
max	maximum value
M	related to mass unit
Me	melting
o	initial or standard value
R	refining

7. References

[1] Němec, L.: Energy consumption in the glass melting process. Pt. 1. Theoretical relations. Glastech. Ber. Glass Sci. Technol. **68** (1995) no. 1, p. 1–10.

[2] Staněk, J: Electric melting of glass. Amsterdam (et al.): Elsevier 1977. p. 365–366.

[3] Němec, L.: Intensification of glass melting by bubbling. Pt. 2. Influence of molten glass stirring on the rate of SiO_2 particles dissolution. (Orig. Czech.) Sklář Keram. **29** (1979) no. 4, p. 103–105.
[4] Němec, L.; Mühlbauer, M.: Verhalten von Gasblasen in der Glasschmelze bei konstanter Temperatur. Glastech. Ber. **54** (1981) no. 4, p. 99–108.
[5] Němec, L.; Schill, P.; Chmelař, J.: Glass refining at reduced pressures. Glastech. Ber. **65** (1992) no. 5, p. 135–141.
[6] Potts, J. C.: A comparison of the rates of melting of some glasses made from sodium carbonate, dolomite limestone and silica sand. J. Soc. Glass Technol. **23** (1939) p. 129–140.
[7] Potts, J. C.: Melting rate of soda–lime–silica glasses as influenced by composition and the effect of minor constituents. J. Am. Ceram. Soc. **24** (1941) no. 2, p. 43–50.
[8] Lyle, A. K.: Melting and fining of sand–soda–lime glasses. In: Trav. IV^e Congrès International du Verre, Paris 1956. p. 93–102.
[9] Němec, L.: Refining in the glassmelting process. J. Am. Ceram. Soc. **60** (1977) no. 9–10, p. 436–440.
[10] Němec, L.; Mühlbauer, M.: Sand concentration distribution over the longitudinal cross section through a glass tank furnace. (Orig. Czech.) Silikáty **27** (1983) no. 4, p. 311–320.
[11] Potts, J. C.; Brookover, G.; Burch, O. G.: Melting rate of soda–lime glasses as influenced by grain sizes of raw materials and by addition of cullet. J. Am. Ceram. Soc. **27** (1944) no. 8, p. 225–231.
[12] Mühlbauer, M.; Němec, L.: Dissolution of glass sand. Am. Ceram. Soc. Bull. **64** (1985) no. 11, p. 1471–1475.

0295P001